Experimental and numerical studies on liquid wicking into filter papers for paper-based diagnostics

Zhi Liu [a, b, 1], Jie Hu [b, c, 1], Yimeng Zhao [a], Zhiguo Qu [a, *], Feng Xu [b, c, **]

[a] Key Laboratory of Thermo-Fluid Science and Engineering of Ministry of Education, School of Energy and Power Engineering, Xi'an Jiaotong University, Xi'an 710049, PR China
[b] Bioinspired Engineering and Biomechanics Center (BEBC), Xi'an Jiaotong University, Xi'an 710049, PR China
[c] The Key Laboratory of Biomedical Information Engineering of Ministry of Education, School of Life Science and Technology, Xi'an Jiaotong University, Xi'an 710049, PR China

HIGHLIGHTS

- A model with considering evaporation was proposed to predict wicking height and mass.
- Flow characteristics of filter paper were experimentally and theoretically studied.
- Effective porosity could be conveniently measured by the experimental platform.
- The evaporation effect tended to reduce the wicking flow speed.

ARTICLE INFO

ABSTRACT

Paper-based diagnostics have shown promising potential applications in human disease surveillance and food safety analysis at the point-of-care (POC). The liquid wicking behavior in diagnostic fibrous paper plays an important role in development of paper-based diagnostics. In the current study, we performed experimental and numerical research on the liquid wicking height and mass with three width strips into filter paper. The effective porosity could be conveniently measured in the light of the linear correlation between wicking height and mass by the experimental system. A modified model with considering evaporation effect was proposed to predict wicking height and mass. The predicted wicking height and mass using the evaporation model was much closer to the experimental data compared with the model without evaporation. The wicking speed initially decreased significantly and then maintained at a constant value at lower level. The evaporation effect tends to reduce the wicking flow speed. More wicking mass could be obtained at larger strip width but the corresponding reagent loss became significant. The proposed model with evaporation paved a way to understanding the fundamental of fluid flow in diagnostic paper and was essential to provide meaningful and useful reference for the research and development of paper-based diagnostics devices.

1. Introduction

Since paper-based analytical devices are simple-to-design, scalable-to-manufacture, inexpensive-to-afford and convenient-to-use, they are uniquely suitable for qualitative and quantitative diagnosis and monitoring of public and global health (e.g., infectious diseases, food safety and water quality) at the point-of-care (POC) [1–4]. In spite of the advantageous features, paper-based diagnostics have been confined by poor sensitivity probably because the underlying mechanism of the fluid flow behavior, such as the speed distribution and the wicking liquid mass in paper remains unclear. Paper-based diagnostics are usually involved in multi-step biochemical processes, and the mixture and interaction time of these reactions are greatly affected by the liquid speed [5]. Meanwhile, there are many influence factors on liquid flow rate in fibrous matrix, such as the characteristics of the substrate (e.g., filter paper) and solution, the dimensions of the channels, evaporation and the environmental temperature and humidity.

* Corresponding author. Tel./fax: +86 (0) 2982668543.
** Corresponding author. Bioinspired Engineering and Biomechanics Center (BEBC), Xi'an Jiaotong University, Xi'an 710049, PR China. Tel./fax: +86 (0) 2982668036.
E-mail addresses: zgqu@mail.xjtu.edu.cn (Z. Qu), fengxu@mail.xjtu.edu.cn (F. Xu).
[1] The authors contributed equally to this work.

Nomenclature

w	The strip width (mm)
δ	The strip thickness (mm)
A	The cross sectional area of paper strip (mm^2)
r	The mean fiber radius (μm)
Δ	The maximum deviation
h_1	The biggest value in Fig. 3(a) (mm)
h_2	One test value in Fig. 3(a) (mm)
h_3	The smallest value in Fig. 3(a) (mm)
h_4	One test value in Fig. 3(a) (mm)
m_{exp}	The wicking liquid mass in experiment (mg)
m_{max}	The maximum measurement range of the electronic balance
h_{exp}	The wicking liquid height in experiment (mm)
h_L	The strip length (mm)
ρ	Density (kg/m^3)
ε	Effective porosity
U_w	Uncertainty of the strip width (mm)
U_δ	Uncertainty of the thickness (mm)
$U_{h_{exp}}$	Uncertainty of the liquid height (mm)
$U_{m_{exp}}$	Uncertainty of the liquid mass (g)
U_ε	Uncertainty of the effective porosity (%)
μ	Viscous (Pa s)
σ	Interfacial tension (N/m)
θ	Contact angle ($^\circ$)

K	Permeability (m^2)
R	The effective pore radius (μm)
h_0	The theoretical liquid wicking height (mm)
S_0	The theoretical liquid speed (mm/s)
m_0	The theoretical liquid wicking height (mg)
t	time (s)
p_w	The water saturated pressure (Pa)
p_v	The partial pressure of vapor in air (Pa)
V_a	The air flow rate (m/s)
γ	The latent heat of vaporization of water (kJ/kg)
φ	The relative humidity
m_{ev}^*	The evaporation rate (mg/(m^2 s))
m_{ev}	The total evaporation mass at every moment (mg)
m_e	The predicted wicking liquid mass (mg)
h_{ev}	The predicted wicking liquid height (mm)
S_{ev}	The predicted liquid speed (mm/s)

Subscript

exp	The experimental result
0	The theoretical value
w	water
v	vapor
a	air
ev	evaporation
e	The predicted value with evaporation

Therefore, it is important to explore these factors in the fluid flow progress in diagnostic paper and it is crucial for designing a paper-based diagnostics to improve the sensitivity by optimizing the assay procedures.

Various methods have been proposed to improve the sensitivity of paper-based diagnostics by changing the flow rate in fibrous matrix, such as changing geometrical structures, adding moderator reagents and so on. For instance, Parolo et al. [6] made a simple change in the architecture of lateral flow assays to alter the fluid speed in different pads and increase the amount of sample, through which they got an 8-fold improvement in sensitivity. Fu et al. [7] investigated T-shape paper networks to achieve multi-step re-actions by changing the length proportion between the two parts with different width in one paper strip. These studies controlled fluid speed in their designs through changing the geometrical structure of paper strips to improve sensitivity. Besides changing paper structure, fibrous matrix of papers can also be modified with hydrophobic material (e.g., paraffin wax) or dissolvable barriers (e.g., glucose and trehalose) to slow down fluid speed directly. For instance, a time-based assay proposed by Noh et al. [8] owned timing function by managing the quantity of wax previously deposited in the paper. Lutz et al. [9] added dissolvable sucrose into paper strips to create flow delays for building the automating multi-step assays protocols. Schilling et al. [10] designed a fully enclosed paper-based devices and found that the amount of toner used to enclose channels could vary the liquid flow rate. Additionally, water soluble pullulan films could serve as a controlled time shutoff system, through which a paper-based device with a time-dependent sequential release of reagents could be made [11] and a hollow channel applied in paper-based devices would enhance the flow rate of solution and reduce the analysis time [12]. However, the above researches just described the qualitative tendency of liquid flow in their devices, most of them might be affected by the evaporation in an open environment. Therefore, the

underlying mechanism with a simplified model still need be further disclosed.

Besides experimental studies, various calculation models had also been developed to reveal the underlying mechanism of fluid flow behavior in essence and to guide the optimization of experiments. Two classical models were frequently used to investigate the characteristics of fluid flow in fibrous material, i.e., Richard's model and Lucas–Washburn model. For instance, Ashari et al. [13,14] combined the Richard's model with Darcy's law to simulate fluid spread in fibrous matrix, however, this model is not appropriate to calculate flow of liquids under saturated conditions as indicated by Richards [15]. In comparison, the Lucas–Washburn model [16] is available for laminar, viscous, incompressible and saturated conditions, but it has not been conformed to situation with evaporation.

In this study, we showed both experiments and simulations to understand fluid flow behavior in filter diagnostic paper. The wicking height and mass at various strip width were experimentally investigated. A modified model with considering the evaporation was built to simulate the flow situation to analyze the flow regularity.

2. Experimental study

2.1. Materials and their physical parameters

A red solution was used to facilitate the observation of experimental phenomena. It was prepared using 0.06 ml of red food additive (Guangzhou Xinde Foods Co., Ltd., China) dissolved in 12 mL of ultrapure water (>18 MΩ) from the Barnstead Nanopure ultrapure water purification system (Thermo Scientific, MA, USA). As the volume fraction of red food additive was only 0.5% in the mixed solution, the physical property parameters of the mixed solution were similar to that of the purified water at the

experimental temperature 20 °C. All the filter papers (qualitative, 102, φ15 mm) used for the preparation of the strip were purchased from Hangzhou Whatman–Xinhua Filter Paper Co., Ltd. (China). The qualitative grade filter paper was cut into 50 mm length of rectangle strips with width of 2 mm, 5 mm and 10 mm by a paper cutter, respectively [Fig. 1(a)]. The average thickness δ of the filter paper was 0.15 mm given by measuring 8 layers of filter paper using a vernier caliper. Therefore, the cross sectional area A of the paper strip was the product of the strip width w and thickness δ ($A = w \cdot \delta$). The mean fiber radius $r(=1.4 \ \mu m)$ could be extracted from a SEM image of filter paper in Fig. 1(b) by averaging multiple measurements.

2.2. Experimental set-up and procedure

Fig. 2 depicts a schematic diagram of the wicking experimental system placed in a closed room. Basically the platform consisted of five parts as follows: an electronic balance to weigh the wicking liquid, a support placed on the electronic balance center, a string to suspend the paper strip above the liquid surface conveniently, a lifting table to control the beginning and end of experiments, and a digital video camera to record the reading of the electronic balance and the wicking liquid front height. The electronic balance was reset to zero before the experiment, thus the electronic balance would display the increased wicking liquid weight directly. The liquid was raised by adjusting the lifting table until the filter paper strip contact with the liquid surface exactly, and the data recording started at the same time as the reading on the electronic balance increased. After a period of time, the lifting table was dropped rapidly until the paper strip separated from the liquid surface.

The wicking liquid experiment data was evaluated from images acquired with the assistance of a digital video camera (Sony HDR-CX510E, Shanghai, China). All the data were obtained from a fixed setting and from the fixed distance. Then, the images observed at different times from the videos were processed with the image processing software Corel DRAW X6. The wicking height and the wicking mass of liquid at each moment were measured from the images.

In the wicking experiments, according to each paper strip with high surface roughness and high distribution of pore size, the in-homogeneity of paper strips might have a negative impact on the accuracy of experiments at the same condition. To identify the in-homogeneity of paper with same pattern, four repeated tests with four paper strips with the same pattern were conducted. Fig. 3(a)
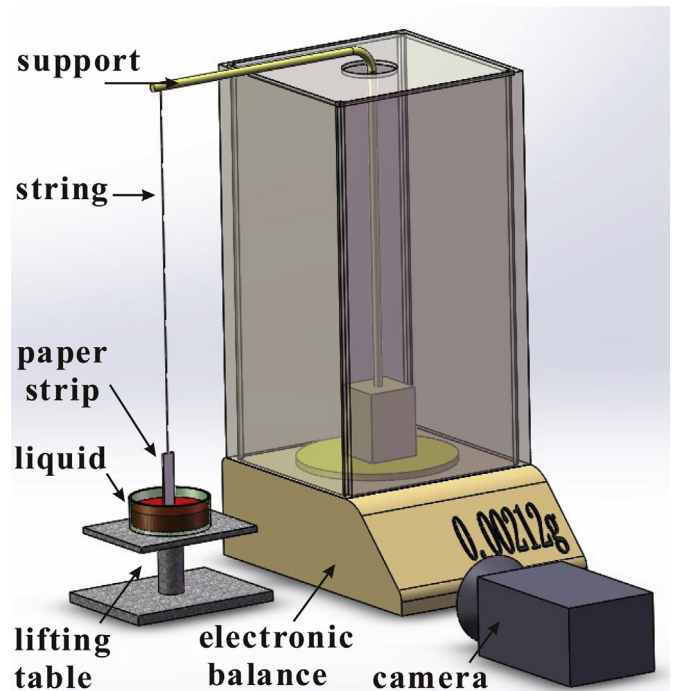

Fig. 2. The experimental set-up.

presents the obtained four wicking heights (h_1, h_2, h_3 and h_4) with 5 mm width paper strips under four repeated tests under same operating conditions. It was found that the deviations between the four heights were small. The values of h_3 and h_1 were found to be the highest and lowest one respectively. As shown in the Fig. 3(b), the maximum deviation [$\Delta = (h_3 - h_1)/h_3 \times 100\%$] was below 10% basically and the deviation of wicking height was less than 2 mm. Therefore the reliability of the experimental system was well confirmed.

2.3. Experimental measurement of effective porosity of filter paper

Fibrous porous materials generally contain open and blocked pores and only the open pores could form connected channels that the fluid can pass through. Hence, the wet area of each cross section excluded the blocked pores was only taken into account. Therefore,
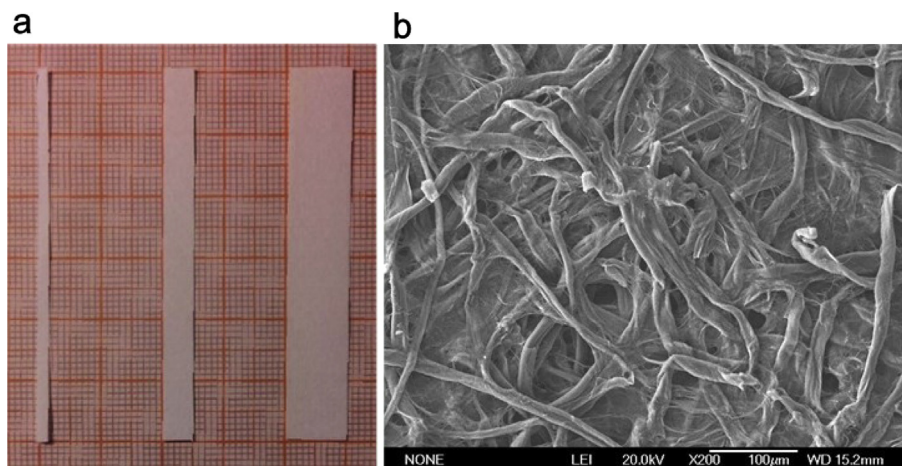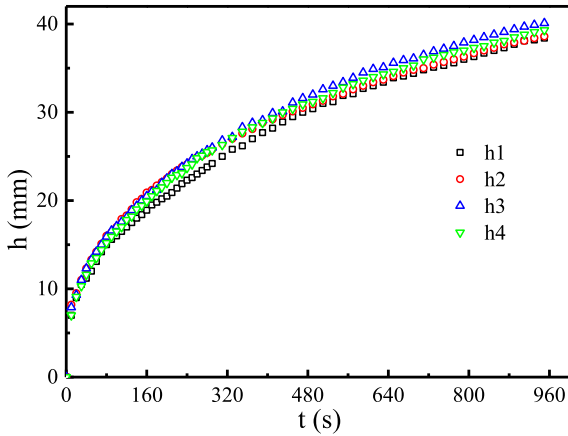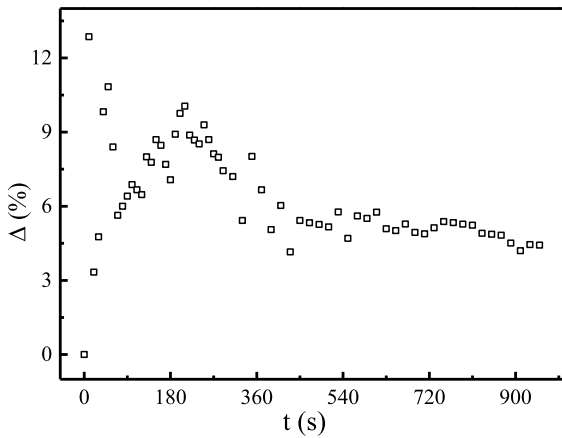

Fig. 1. The filter paper. (a) Paper strip, (b) SEM image of the filter paper.

(a) Correlation between the wicking height and time in a repeat experiment (w=5mm)

(b) The maximum deviation of the four experiments

Fig. 3. The reliability of the experimental system.

the experimentally measured porosity in the present study can be considered as a kind effective porosity in the wet situation Based on the defined effective porosity, the liquid mass and height satisfy the linear relationship shown in Eq. (1):

$$m_{exp} = \rho \varepsilon A h_{exp} = \rho \varepsilon w \delta h_{exp} \tag{1}$$

where, m_{exp}, ρ, ε, h_{exp}, A, w and δ are liquid mass, density, effective porosity, wicking liquid height, cross sectional area of the paper strip, strip width and thickness, respectively. Indeed, the absolute porosity and the cross-sectional area may vary before and after saturation, which would have an influence on this linear relationship shown in Eq. (1). For example, the cross-sectional area A may have a tiny change before and after saturation on account of that the swelling was about 3% of the total paper thickness as indicated by Lioumbas et al. [17]. Thus the change of the cross-sectional area could be ignored. In the present study, the existence effects of blocked pores, the variation of porosity and cross-sectional area in fibrous materials were taken into account within the effective porosity. Therefore, the effective porosity of the filter paper could be measured directly through the linear relationship shown in Eq. (1). Fig. 4 shows a good linear relationship between the wicking height and mass for 5 mm width paper strip. The filter paper effective porosity was obtained as 0.69 based on the slope of the fitting curve (0.515) as well. An uncertainty analysis conducted for the strip width U_w, thickness U_δ, liquid height $U_{h_{exp}}$, liquid mass

$U_{m_{exp}}$ and the effective porosity U_ε was summarized in Table 1, respectively. The type An uncertainties of the strip width U_w and thickness U_δ could be calculated with the values of 8 measurements directly. They were 0.5 mm and 0.007 mm, respectively. The liquid front may not be a horizontal line, and the liquid height observed from the video is averaged over the width of paper strip, meanwhile, the maximum error of liquid height $U_{h_{exp}}$ is less than 2 mm apparently in the video. The uncertainty for the liquid mass $U_{m_{exp}}$ was 1.0×10^{-4} g corresponding to the precision of electronic balance. Thus, the uncertainty for the effective porosity U_ε was determined to be 11.7% based on the uncertainties of U_w, U_δ, $U_{h_{exp}}$, $U_{m_{exp}}$, the strip length h_L and maximum measurement range of the electronic balance m_{max} according to Eq. (1).

3. Numerical methods

3.1. A review of model without considering evaporation

The liquid can transport through the filter paper strip slowly under the effect of capillary force, inertial force, viscous resistance and gravity. Fries [18] analyzed the analytical solution, and found that inertial force and gravity can be neglected. For capillary flow in porous materials, Lucas–Washburn equation [16] proposed a model based on the momentum balance including only viscous resistance and capillary force, and the formula was shown in Eq. (2a):

$$h_0 = \sqrt{\frac{4\sigma \cos(\theta)}{\mu} \frac{K}{\varepsilon R}} \cdot t^{1/2} \tag{2a}$$

The corresponding liquid speed was then defined as:

$$S_0 = \frac{dh_0}{dt} = \sqrt{\frac{\sigma \cos(\theta)}{\mu} \frac{K}{\varepsilon R}} \cdot t^{-1/2} \tag{2b}$$

In Eqs. (2a) and (2b), h_0, S_0, σ, μ, θ, K, R, t are theoretical wicking liquid front height, theoretical liquid speed, interfacial tension, viscous, contact angle, permeability, the effective pore radius and the time, respectively.

The interfacial tension and viscous can be obtained from the physical property parameters of water. The contact angle θ
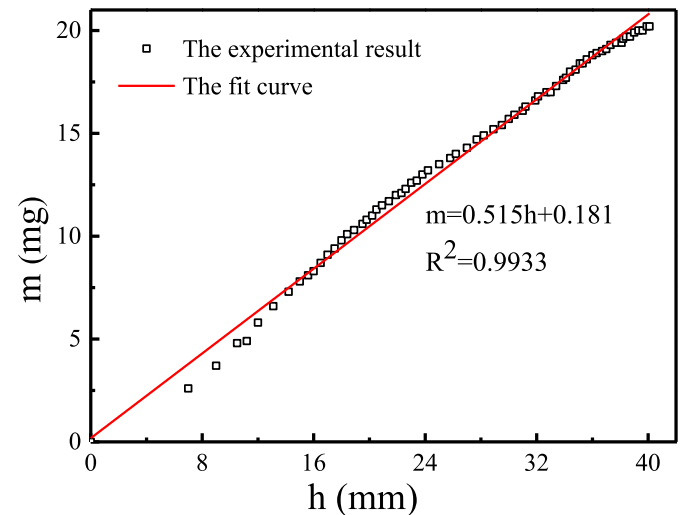
Fig. 4. Correlation of liquid mass inside the strip and the wicking height ($w = 5$ mm).

Table 1
Uncertainties for measured variables.

Variable	Formula	Parameters	Uncertainty
Strip width	$U_w = \sqrt{\frac{\sum (w_i - \overline{w})}{n(n-1)}}$	$U_w = 0.5$ mm	0.5 mm
Thickness	$U_\delta = \sqrt{\frac{\sum (\delta_i - \overline{\delta})}{n(n-1)}}$	$U_\delta = 0.5$ mm $n = 8$	0.007 mm
Liquid height		$U_{h_{exp}} = 2$ mm	2 mm
Liquid mass		$U_{m_{exp}} = 1.0 \times 10^{-4} g$	1.0×10^{-4} g
Effective porosity	$U_\varepsilon = \sqrt{\left(\frac{U_w}{w}\right)^2 + \left(\frac{U_\delta}{\delta}\right)^2 + \left(\frac{U_{h_{exp}}}{h_L}\right)^2 + \left(\frac{U_{m_{exp}}}{m_{max}}\right)^2}$	$w = 5$ mm $\delta = 0.15$ mm $h_L = 50$ mm $m_{max} = 100$ g	11.7%

quantified by Young equation is not always unique because of plenty influence factors, such as temperature, equilibration time, roughness and so on as indicated by Yuan et al. [19]. Therefore, the contact angle θ was assumed to 80° according to Lu and co-author's research [20]. The permeability K is an important parameter of filter paper in practical application. It shows a measure of the ability of a porous matrix to transmit fluids. Kozeny–Carman correlation [21] is an empirical equation to predict the permeability, however it is just suitable for the isotropic fibrous material as indicated in Ref. [22]. Van der Westhuizen et al. [23] developed a mathematic solution of the phase average Navier Stokes equation for the orthotropic (transverse) permeability of random unidirectional fiber beds. The permeability of filter paper was calculated from Eq. (3) by Van der Westhuizen et al. [23].

$$K = r^2 \frac{\pi \varepsilon \left(1 - \sqrt{1 - \varepsilon}\right)^2}{24(1 - \varepsilon)^{1.5}} \tag{3}$$

In Eq. (4), the pore radius R was carried out from the correlation of Tomadakis et al. [24] in which the pore radius R and the mean fiber radius r limited to randomly overlapping fiber structures was correlated. The formula was expressed as:

$$R = \frac{-r}{\ln \varepsilon} \tag{4}$$

The values of geomantic parameters, the width w and the thickness δ, the mean fiber radius r, the effective pore radius R, effective porosity ε and the values of physical parameters, the density ρ, the viscous μ, interfacial tension σ, permeability K were summarized in Table 2 and Table 3, respectively.

Similar to Eq. (1), the theoretical wicking fluid mass m_0 was expressed as:

$$m_0 = \rho \varepsilon w \delta h_0 \tag{5}$$

where, the theoretical wicking fluid mass was composed of the actual liquid mass and the evaporation mass. To get the correlation between the theoretical wicking mass and time, Eq. (2) was substituted in Eq. (5), resulting in

$$m_0 = \rho w \delta \sqrt{\frac{4\sigma \cos(\theta)}{\mu} \frac{K}{R} \varepsilon} \cdot t^{1/2} \tag{6}$$

3.2. A modified model with considering evaporation

The classical mathematical model [Eq. (2)] only considered viscous resistance and capillary force, it ignored the evaporation for a long time at an open space. Jahanshahi-Anbuhi et al. [11] used a correlation to calculate the water evaporation rate at each relative humidity from the ASHRAE handbook, as:

$$m_{ev}^* = (p_w - p_v) \times \frac{(0.089 + 0.0782 V_a)}{\gamma} \tag{7}$$

where m_{ev}^*, p_w, p_v, V_a, γ are the evaporation rate, water saturated pressure, the partial pressure of vapor in air, air flow rate, the latent heat of vaporization of water, respectively. The relative humidity φ is defined as a radio of the partial pressure of vapor in air and water saturated pressure at fixed pressure and temperature. The definition of relative humidity was given as:

$$\varphi = \frac{p_v}{p_w} \tag{8}$$

The Eq. (7) was rewritten as:

$$m_{ev}^* = (1 - \varphi) \times p_w \times \frac{(0.089 + 0.0782 V_a)}{\gamma} \tag{9}$$

The experiment was carried out in a closed room, the air flow speed V_a was assumed to be zero and the relative humidity φ was tested with a moisture meter as 52%. The values of p_w and γ are 2338 Pa and 2454.3 kJ/kg according to the physical properties of dry air and water at fixed temperature 20 °C. As a result, the evaporation rate was determined as a constant value of 0.0407 g/(m² s). In the evaporation model, the total evaporation mass m_{ev} (ignoring the area on the thickness direction) at every moment could be calculated through the integral formula:

$$m_{ev} = \int_0^t m_{ev}^* \cdot 2 \cdot w \cdot h_{ev} dt \tag{10}$$

where, h_{ev} is the predicted wicking liquid height. Therefore, the predicted wicking liquid mass m_e at every moment was the difference between the theoretical value m_0 and the evaporation mass m_{ev}, as:

Table 2
The geometrical parameters of filter paper.

Parameter	w (mm)	δ (mm)	r (μm)	R (μm)	ε
Value	2.0/5.0/10.0	0.15	1.4	3.77	0.69

Table 3
The physical parameters.

Parameter	ρ (kg/m³)	μ (Pa s)	σ (N/m)	K (m²)
Value	998.2	1004.0×10^{-6}	726.9×10^{-4}	2.01×10^{-13}

$$m_e = m_0 - m_{ev} = \rho w \delta \sqrt{\frac{4\sigma \cos(\theta)}{\mu} \frac{K}{R} \varepsilon} \cdot t^{1/2} - \int_0^t m_{ev}^* \cdot 2 \cdot w \cdot h_{ev} dt \tag{11}$$

Meanwhile, the predicted wicking liquid mass m_e at every moment could be obtained by the wicking liquid density and its volume, expressed as:

$$m_e = \rho \varepsilon w \delta h_{ev} \tag{12}$$

As a consequence, the predicted wicking liquid height could be written as:

$$h_{ev} = \frac{m_e}{\rho \varepsilon w \delta} = \sqrt{\frac{4\sigma \cos(\theta)}{\mu} \frac{K}{\varepsilon R}} \cdot t^{1/2} - \frac{2m_{ev}^*}{\rho \varepsilon \delta} \int_0^t h_{ev} dt \tag{13}$$

By differential calculation method, the Eq. (13) was recast in Eq. (14a) and its definite condition was also provided in Eq. (14b):

(a) Wicking height versus time curve

(b) The wicking liquid speed versus time curve

Fig. 5. Characteristic of liquid flow ($w = 5$ mm).

$$\frac{dh_{ev}}{dt} = N \cdot t^{-1/2} - M \cdot h_{ev} \tag{14a}$$

$$h_{ev} = 0, \quad t = 0 \tag{14b}$$

where:

$$M = \frac{2m_{ev}^*}{\rho \varepsilon \delta}, \quad N = \sqrt{\frac{\sigma \cos(\theta)}{\mu} \frac{K}{\varepsilon R}} \tag{14c}$$

Eq. (14a) was a first order ordinary differential equation and its solution was expressed in Eq. (15):

$$h_{ev} = 2N \cdot e^{-Mt} \int_0^{\sqrt{t}} e^{Mt^2} dt \tag{15}$$

The corresponding predicted wicking speed S_{ev} was expressed as:

$$S_{ev} = \frac{dh_{ev}}{dt} = N \cdot t^{-1/2} - 2M \cdot N \cdot e^{-Mt} \int_0^{\sqrt{t}} e^{Mt^2} dt \tag{16}$$

The second term with variable upper limit integral was non-integrable, we employed the numerical integration to calculate the predicted wicking liquid height. Then the total evaporation mass, the predicted wicking liquid mass and the liquid speed could be calculated through numerical iterative method in turn. It was noted that the predicted wicking height was irrelevant to strip width as indicated in Eq. (15), whereas, the wicking mass was obviously dependent on strip width.

4. Results and discussion

4.1. Effect of evaporation on liquid wicking

The predicted wicking height, wicking speed and wicking mass predicted by evaporation model and conventional model without evaporation were compared with experimental data. The wicking height and wicking liquid speed between experiment data and different calculation models with 5 mm width paper strips were compared in Fig. 5(a) and (b), respectively. As shown in Fig. 5(a), the predicted wicking height with considering evaporation agreed well with the experimental data, whereas the deviations between the predicted wicking height without considering evaporation and experimental data were obvious. This implied the feasibility to consider the evaporation effect. As shown in Fig. 5(b), the experimental wicking liquid speed was average value, which was the ratio between two adjacent wicking height and time difference. The liquid speed for models with and without evaporation was obtained by the Eq. (2b) and Eq. (16), respectively. The liquid speed decreased rapidly at first and this decrease trend became insignificant after a period of time. Again, better agreement between experimental data and theoretical with considering the evaporation effect model was achieved. The liquid speed in the model with considering evaporation was lower than that in the model without considering evaporation because the water molecules diffused out of the paper surface and horizontal migration of water occurred. Then, the evaporation creates a negative effect on the capillarity to reduce the wicking fluid speed. These results revealed that the evaporation was a critical factor to slow down the fluid speed and the suppression trend for speed increasing and this effect became more obvious as time increased.
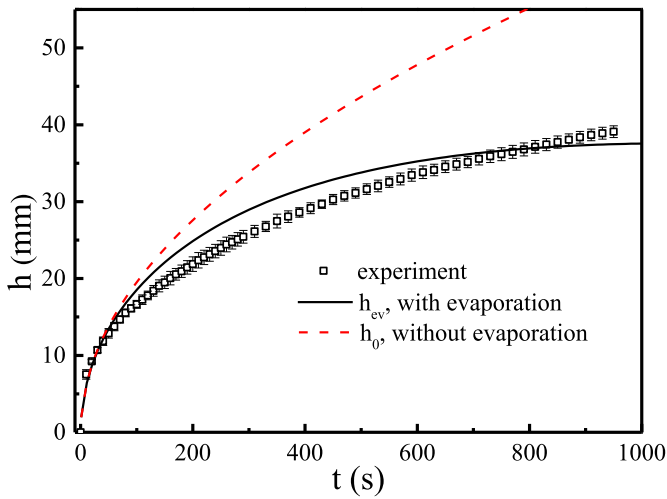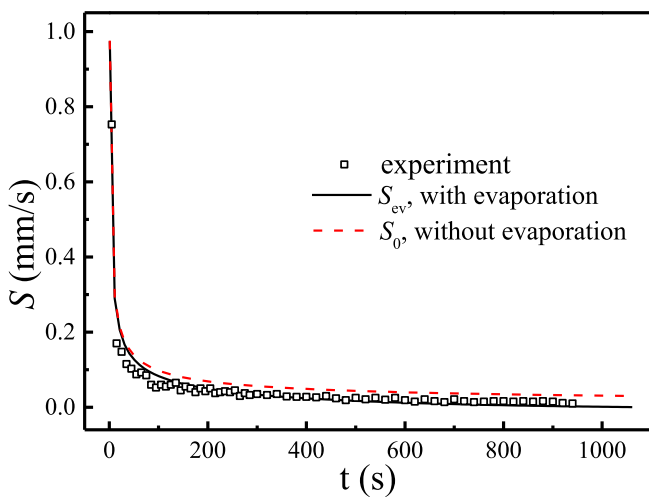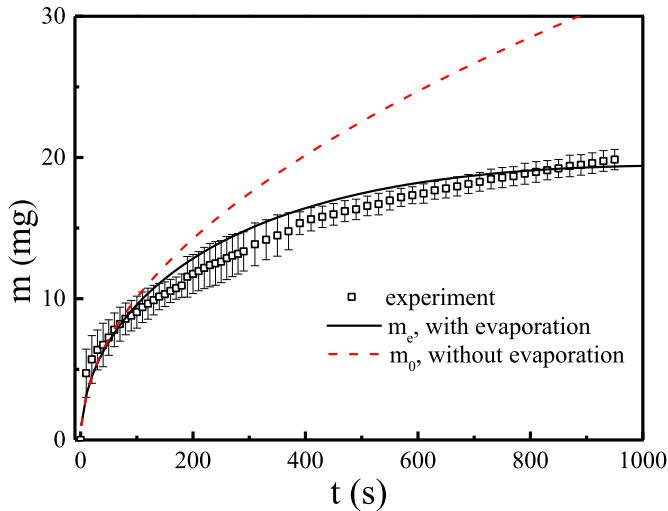
Fig. 6. Wicking mass versus time curve ($w = 5$ mm).

Fig. 8. Comparison of wicking mass at different strip width.

Fig. 6 depicts the comparison for the wicking mass versus time between experiment data and different calculation models with 5 mm paper strips. The difference of wicking mass between the calculation result without considering evaporation and the experiment data gradually became more significant with elapse of time. Comparatively, the calculation result with considering evaporation agreed well with the experimental data. Therefore, the feasibility of present model was validated in actual engineering application.

4.2. Effect of strip's width on liquid wicking

Figs. 7 and 8 compared the wicking height and mass between experimental data and prediction with evaporation model at three different width strips, respectively. The strip width has no impacts on the wicking height as indicated in Eq. (15) because the paper width could be considered as infinite width and the boundary effects were not considered. Whereas, the experimental results with different strip widths had mild difference and the wicking height increased with an increase in strip width as shown in Fig. 7. Hence, it was speculated that the boundary effect for wider width was weaker than that for smaller width. Generally, the predicted wicking height agreed well with the experimental data. The wicking mass obviously increased with an increase in strip width as
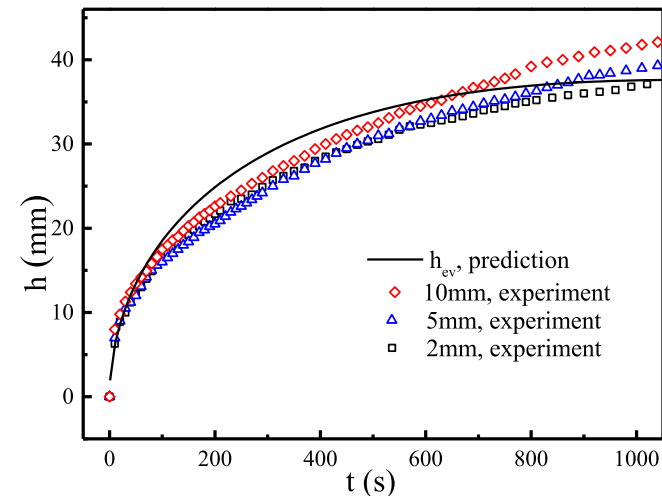
also shown in Fig. 8 and indicated in Eq. (11). This implied that more sample volume could exist in the reaction in paper-based diagnostics and this occurrence might make a contribution to a stronger signal. On the other hand, more liquid will lost caused by the evaporation for a strip with larger width under a long time period of time. Therefore, it is necessary to select an appropriate width when paper-based diagnostics is developed.

5. Conclusions

A liquid wicking experiment platform was built to investigate flow characteristics of filter paper strip. The wicking height and mass at three different width strips was experimentally investigated. The effective porosity could be conveniently measured by the linear correlation between wicking height and mass. A modified mathematical model with considering the evaporation was proposed to predict the wicking height and mass for fibrous porous strip. The simulated wicking height and mass with evaporation model agreed well with experimental data. The occurrence of evaporation tended to slow down the fluid speed. The wicking height with larger strip width was a little higher than that with smaller strip width because of boundary effect. The filter strip with higher width could wick larger volume liquid but consumed more reagent through the evaporation. The mathematical model was expected to provide optimization and improvement of paper-based diagnostics development.

Acknowledgements

Fig. 7. Comparison of wicking height at different strip width.

References

[1] A.W. Martinez, S.T. Phillips, G.M. Whitesides, E. Carrilho, Diagnostics for the developing world: microfluidic paper-based analytical devices, Anal. Chem. 82 (2009) 3–10.

[2] W.G. Lee, Y.-G. Kim, B.G. Chung, U. Demirci, A. Khademhosseini, Nano/Microfluidics for diagnosis of infectious diseases in developing countries, Adv. Drug. Deliv. Rev. 62 (2010) 449–457.

[3] C. Rivet, H. Lee, A. Hirsch, S. Hamilton, H. Lu, Microfluidics for medical diagnostics and biosensors, Chem. Eng. Sci. 66 (2011) 1490–1507.

[4] J. Hu, S. Wang, L. Wang, F. Li, B. Pingguan-Murphy, T.J. Lu, et al., Advances in paper-based point-of-care diagnostics, Biosens. Bioelectron. 54 (2014) 585–597.

[5] H. Noh, S.T. Phillips, Metering the capillary-driven flow of fluids in paper-based microfluidic devices, Anal. Chem. 82 (2010) 4181–4187.

[6] C. Parolo, M. Medina-Sánchez, A. de la Escosura-Muñiz, A. Merkoçi, Simple paper architecture modifications lead to enhanced sensitivity in nanoparticle based lateral flow immunoassays, Lab. Chip 13 (2013) 386–390.

[7] E. Fu, S. Ramsey, P. Kauffman, B. Lutz, P. Yager, Transport in two-dimensional paper networks, Microfluid Nanofluid 10 (2011) 29–35.

[8] H. Noh, S.T. Phillips*, Fluidic timers for time-dependent, point-of-care assays on paper, Anal. Chem. 82 (2010) 8071–8078.

[9] B. Lutz, T. Liang, E. Fu, S. Ramachandran, P. Kauffman, P. Yager, Dissolvable fluidic time delays for programming multi-step assays in instrument-free paper diagnostics, Lab. Chip 13 (2013) 2840–2847.

[10] K.M. Schilling, A.L. Lepore, J.A. Kurian, A.W. Martinez, Fully enclosed microfluidic paper-based analytical devices, Anal. Chem. 84 (2012) 1579–1585.

[11] S. Jahanshahi-Anbuhi, A. Henry, V. Leung, C. Sicard, K. Pennings, R. Pelton, et al., Paper-based microfluidics with an erodible polymeric bridge giving controlled release and timed flow shutoff, Lab. Chip 14 (2014) 229–236.

[12] C. Renault, X. Li, S.E. Fosdick, R.M. Crooks, Hollow-channel paper analytical devices, Anal. Chem. 85 (2013) 7976–7979.

[13] A. Ashari, T.M. Bucher, H.V. Tafreshi, M.A. Tahir, M.S.A. Rahman, Modeling fluid spread in thin fibrous sheets: effects of fiber orientation, Int. J. Heat. Mass Transf. 53 (2010) 1750–1758.

[14] A. Ashari, T.M. Bucher, H.V. Tafreshi, Modeling motion-induced fluid release from partially saturated fibrous media onto surfaces with different hydro-philicity, Int. J. Heat. Fluid Flow. 32 (2011) 1076–1081.

[15] L.A. Richards, Capillary conduction of liquids through porous mediums, J. Appl. Phys. 1 (1931) 318–333.

[16] E.W. Washburn, The dynamics of capillary flow, Phys. Rev. 17 (1921) 273–283.

[17] J.S. Lioumbas, A. Zamanis, T.D. Karapantsios, Towards a wicking rapid test for rejection assessment of reused fried oils: results and analysis for extra virgin olive oil, J. Food Eng. 119 (2013) 260–270.

[18] N. Fries, Capillary Transport Processes in Porous Materials: Experiment and Model, Cuvillier, Göttingen, 2010, pp. 77–113.

[19] Y. Yuan, T.R. Lee, Contact angle and wetting properties, in: G. Bracco, B. Holst (Eds.), Surface Science Techniques, Springer, Berlin Heidelberg, 2013, pp. 3–34.

[20] Z. Lu, P. Anne, L. Maryline, C. Christine, Wetting behavior of thermally bonded polyester nonwoven fabrics: the importance of porosity, J. Appl. Polym. Sci. 102 (2006) 387–394.

[21] M.M. Tomadakis, Viscous permeability of random fiber structures: comparison of electrical and diffusional estimates with experimental and analytical results, J. Compos. Mater. 39 (2005) 163–188.

[22] B.R. Gebart, Permeability of unidirectional reinforcements for RTM, J. Compos. Mater. 26 (1992) 1100–1133.

[23] J. Van der Westhuizen, J. Prieur Du Plessis, An attempt to quantify fibre bed permeability utilizing the phase average Navier-Stokes equation, Compos. Part A: Appl. Sci. Manuf. 27 (1996) 263–269.

[24] M.M. Tomadakis, S.V. Sotirchos, Effective Kundsen diffusivities in structures of randomly overlapping fibers, AIChE J. 37 (1991) 74–86.